Cortical beta power reflects a neural implementation of decision boundary collapse in a speeded flanker task

Hans Kirschner[1]*, Adrian G. Fischer[2]*, Claudia Danielmeier[3], Tilmann A. Klein[1,4,5] and Markus Ullsperger[1,4]

[1]Institute of Psychology, Otto-von-Guericke University, D-39106 Magdeburg, Germany. [2]Department of Education and Psychology, Freie Universität Berlin, D-14195 Berlin, Germany. [3]School of Psychology, University of Nottingham, Nottingham NG7 2RD, UK. [4]Center for Behavioral Brain Sciences, D-39106 Magdeburg, Germany. [5] Department of Neurology, Max Planck Institute for Human Cognitive and Brain Sciences, D-04103 Leipzig, Germany.

*equal contribution

Abstract

A prominent account of decision-making assumes that information is accumulated until a fixed response threshold is crossed. However, many everyday decisions require weighting of information appropriately against time. Collapsing response thresholds are a mathematically optimal solution to this decision problem. However, evidence in favour of dynamic response thresholds and a neural implementation thereof is sparse. Here, we investigated whether lateralization of EEG beta power can demonstrate a plausible neural mechanism for collapsing decisions thresholds in a large sample of 863 healthy participants who completed a speeded flanker task. We show that a multistage drift diffusion model with dynamic decision thresholds explained participants behaviour better than a model with fixed thresholds. Predictions of the dynamic decision threshold model were reflected in the beta band signal, where slower responses show a decreased beta power lateralisation (BPL). These data suggest that peak BPL, coinciding with the motor response, may serve as a neural proxy for the decision threshold.

Introduction

We often make decisions under time pressure, precluding extensive evidence accumulation in favour of or against choice alternatives. Imagine, for example, a basketball player who must trade off the accuracy of a shoot against the amount of available time as a defender approaches. Psychology and neuroscience have successfully utilized sequential sampling models such as the drift-diffusion model (DDM) to understand the underpinnings of decision-making (Ratcliff et al., 2016). DDMs assume that decisions are triggered when the accumulated evidence for one option/alternative crosses a response threshold. Traditionally, diffusion models assume a time-invariant decision policy, which is reflected in fixed decision boundaries. However, as in the example above, this assumption may be ill-posed on situations where decisions must be made under time pressure. Consequently, more recently, diffusion models with collapsing decision bounds gained popularity (Hawkins, Forstmann, et al., 2015; Palestro et al., 2018; Ratcliff et al., 2016). Here, as time passes, decisions are triggered at decreasing decision thresholds. This facilitates terminating decision making when no solution can be reached within the desired time frame.

While collapsing decision boundaries are a mathematically optimal solution to the decision problem, except for some evidence in monkeys (Purcell & Kiani, 2016), no neural data has confirmed a neural implementation of dynamic boundaries yet (Hanks & Summerfield, 2017; Thura & Cisek, 2017). It has recently been suggested that the motor cortex is involved in the decision-making process by continually sampling information in favour or against response options (Cisek & Kalaska, 2005; Pape & Siegel, 2016). In the EEG, this process is reflected in beta band (13-25 Hz) activity over centroparietal electrodes. It has been shown that beta power over the contralateral motor-cortex decreases before any overt action and even reflects imaginary movements (Kuhn et al., 2006). The difference in beta

power between both motor-cortices may thus encode the relative evidence in favour of respective response options in a lateralised fashion (Donner et al., 2009; Pape & Siegel, 2016), or, put more broadly, decisions in action-space (Cisek & Kalaska, 2005; Hunt et al., 2013). In this line of research, we recently demonstrated that model parameters of a multistage drift-diffusion model and the lateralisation of EEG beta power convergently show a complex interplay that facilitates behaviour adaptations after erroneous responses in a flanker task (Fischer et al., 2018). Specifically, suppression of distracting evidence, together with increased response thresholds appear to cause slower and more accurate post-error responses. Based on this work demonstrating a remarkable similarity of the time course of the decision variable in the DDM and the beta power lateralization (BPL) over motor cortex, we argue that the pre-response BPL peak can serve as a proxy for response thresholds.

Here, we follow-up on this argumentation and investigate whether BPL can demonstrate a plausible neural mechanism for collapsing decision thresholds in a large sample of 863 healthy participants. We complemented our previous multistage DDM by an additional free parameter that allowed decision bounds to collapse according to a cumulative Weibull distribution. As depicted in Figure 1B, this model makes distinct predictions about the decision threshold depending on speed: later decisions are made at a lower threshold. We hypothesized that this decision threshold collapse would also be reflected in the decreased BPL for slower responses. Indeed, we found that the extended DDM provides a better fit for the data. This model predicts decision threshold differences due to boundary collapse over time. This is confirmed in the beta band signal, where slower responses show a decreased BPL. These data suggest that peak BPL, coinciding with the motor response, may serve as a neural proxy for the decision threshold.

Results and Discussion

Eight hundred and sixty-three healthy subjects performed a speeded arrow-version of an Eriksen flanker task while EEG was recorded. Participants were instructed to respond as quickly and accurately as possible to the direction of a centrally presented arrow (see Figure 1A). To elicit a large proportion of response errors, we presented distracting flanking stimuli in visual proximity and slightly ahead in time (83 ms) of the imperative, central target stimulus. On incongruent stimulus sets a mismatch between the flanker and target arrow directions induced conflicting response tendencies. The response conflict was further enhanced by manipulation of stimulus distances among each other (close and far, Danielmeier et al. (2009)) and response-stimulus intervals (short and long, Danielmeier and Ullsperger (2011)). To increase time-pressure, we kept the response stimulus intervals (RSIs) and the response window of 1200 ms rather short. Behavioural analyses of this task confirmed that general behaviour effects were in accordance with typical results seen in flanker tasks. They reflected interference effects, with slower ($\Delta RT = + 62$ ms, $t(862) = -81.79$, $p < .001$, $d = 1.03$, $BF_{10} = \infty$) and more erroneous ($\Delta accuracy = 20\%$, $t(862) = 96.18$, $p < .001$, $d = 3.44$, $BF_{10} = \infty$) responses on incongruent trials, whereby these effects interacted with flanker distance. Moreover, all error-related behavioural adaptations associated with cognitive control (post-error slowing (PES), post-error increase in accuracy (PIA), post-error reduction on interference (PERI)) were present. Overall participants responded accurately (mean accuracy > 85%) and errors were committed at faster RT compared to hits (see Fischer et al., 2018 for a detailed description of these results).

An extended DDM with collapsing decision boundaries captures task behaviour best

We have previously shown that an extended multistage DDM captures these behavioural effects (Fischer et al., 2018). In brief, this model assumes that choice options are mutually exclusive, so that a single decision variable is reflecting both decision options. Features of the DDM are depicted in Figure 1B. On every trial, the decision can be randomly biased slightly to one response option (startpoint variance, sz). The height of the boundary parameter (a) determines how much evidence accumulation is required to cross the boundary and trigger a response. The non-decision time parameter (T_{er}), reflects the time from actual flanker onset until the information can be used to influence the decision process, which in our model can vary from trial to trial (st). During flanker-only presentation, evidence was accumulated in the direction of the flankers (83 ms). After target onset, evidence accumulation is driven by the direction of the target. We demonstrated that a model that allowed for trial-by-trial weighting of the distractor-driven diffusion (simulating an attentional process suppressing the influence of the flankers) explained participants' behaviour best. Comparisons of model estimates fitted to either post-error or post-correct trials revealed that post-error adaptations are facilitated by a complex interplay of multiple mechanisms: suppression of distracting evidence, response threshold increase, and reduction of evidence accumulation. To investigate whether dynamic decision boundaries explain subjects' behaviour better, we complemented the multistage DDM described previously by an additional free parameter that scaled decision bound collapse according to a cumulative Weibull distribution. As can be seen in Figure 1B, this model makes a specific prediction: later decisions are formed at a lower threshold. Model comparison (Figure 2A) revealed that our data is better described by the collapsing bound model than by the original models (described in the method section). This indicates that individuals apply a discounting function that decreases decision thresholds when time is

running out (i.e., the response window of 1200 ms closes). Overall, the model provided a good fit to the data and matched participants RTs and accuracies (Figure 2B and 2C). Parameter recovery studies suggest that this model was capable to reliably recover parameters that generated synthetic data (see supplementary Figure 1). When averaged across trials, threshold differences are clearly visible, whereby fast responses show a higher threshold (Figure 2E and 2F). Interestingly, our results are at odds with previous research identifying evidence in favour of standard DDMs with fixed bounds in humans (Hawkins, Forstmann, et al., 2015; Hawkins, Wagenmakers, et al., 2015; Ratcliff et al., 2016). In these studies, other decision-making tasks were used (i.e., random dot motion, brightness discrimination, dot separation) and DDMs treat (perceptual) interference trials as trials on which drift rates are low to capture the increased RT and uncertainty on (error)-trials. However, lower drift rates per trial cannot produce fast errors. Yet, fast errors are a hallmark of speeded reaction time tasks, like our flanker task. Here, fast errors arise from an interaction of distractor-driven biasing and trial-wise pre-lateralization of the decision variables as well as noise during stimulus processing (Fischer et al., 2018). Moreover, in contrast to most other decision-making tasks, after flanker and target presentation (which was only presented for 33 ms in our task) no further information could be sampled to inform decisions. Thus, decision policies might be task-dependent and affected by various factors.

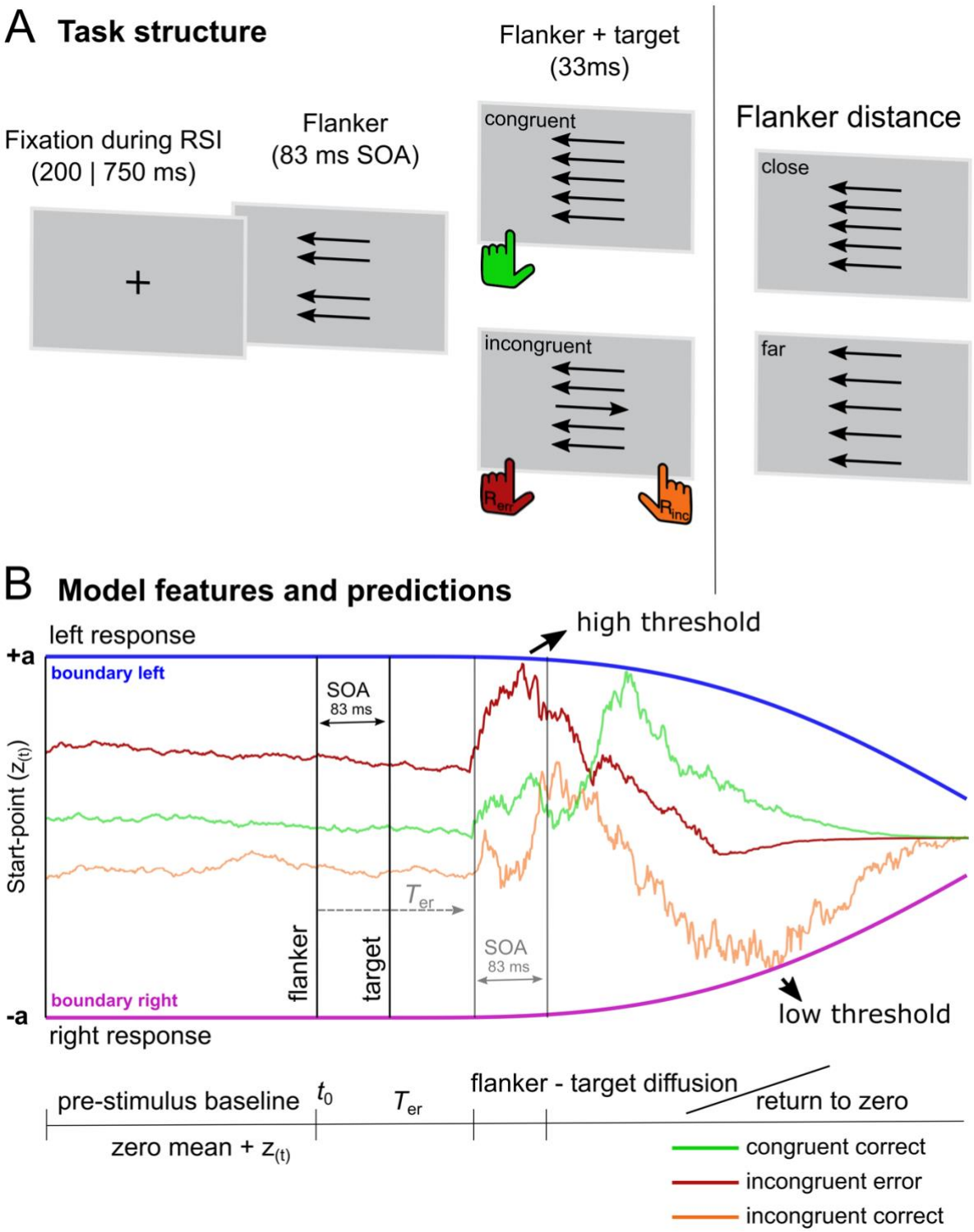

Figure 1. Task information, model features and predictions.

(A) In the flanker task either congruent or incongruent flankers (four surrounding arrows) in proximity or further away from the central target (inlet) are presented on each trial. Congruent stimuli usually yield faster responses (green) compared to incongruent stimuli, which lead to delayed responses (orange) or induce errors (red). **(B)** Illustration of the multi-stage DDM. On a given trial, the decision can be randomly biased to favour one response (startpoint variance, sz). The height of the boundary

(Figure 1 continued) parameter (a) determines how much evidence accumulation is required to cross the boundary and trigger a response. Finally, visual processing and motor execution times are captured by the non-decision time (T_{er}) parameter, which in our model can vary from trial to trial (st). Evidence accumulation followed the flankers' direction during the time they were displayed on screen alone (83 ms). After target onset, evidence accumulation was driven by the direction of the target.

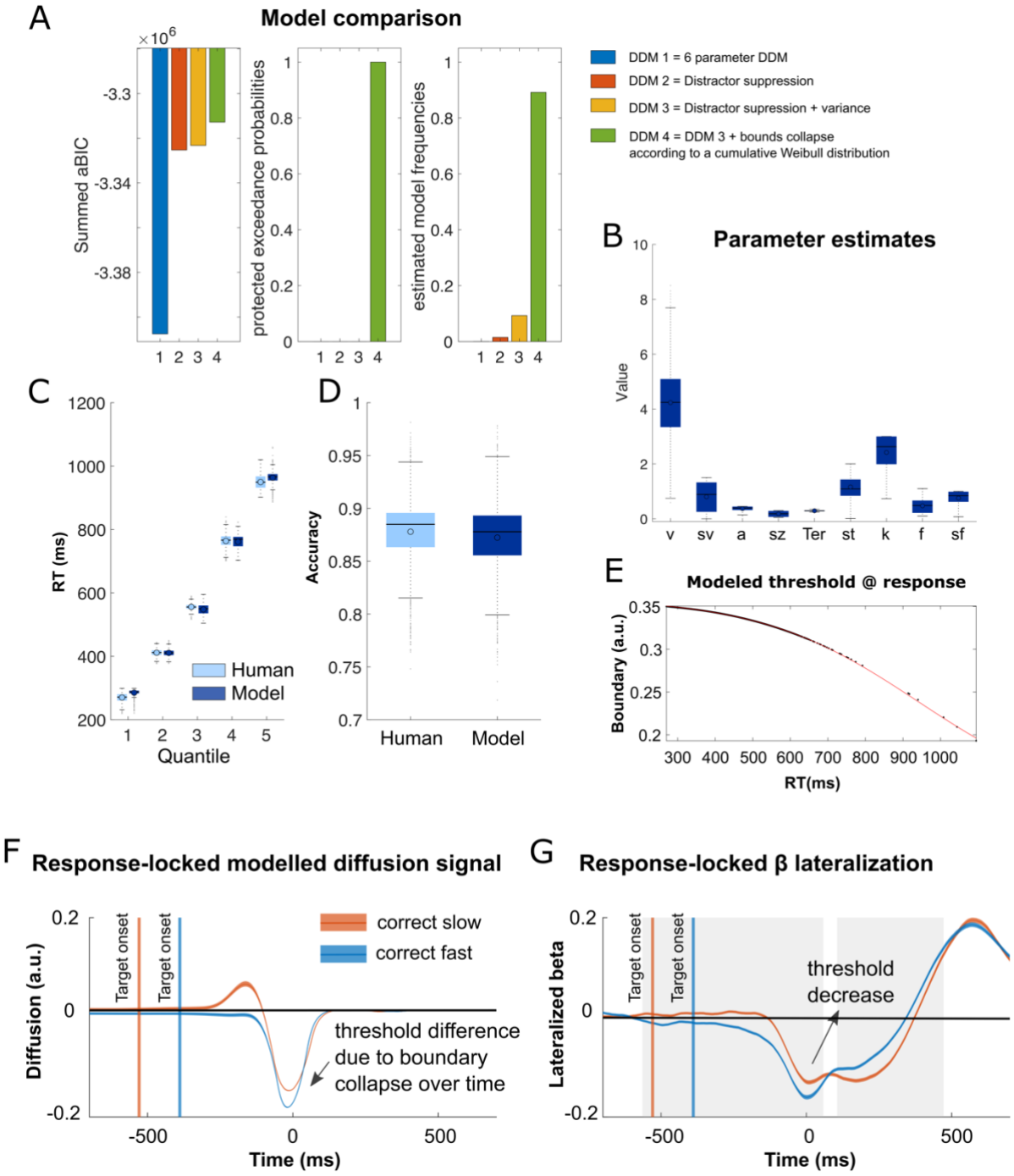

Figure 2. Drift-diffusion model fits and model and empirical decision signals.

(A) Cumulated approximated Bayesian Information Criterion (aBIC) scores over participants of each candidate model. Higher values indicate a better fit of the models to the behavioral data. Results indicate that the dynamic bound model (DDM4) provides the best fit to the data. Protected exceedance probabilities (pEP) similarly favor DDM 4. **(B – D)** Model 4 provides a good fit to the data and matches participants' RTs and accuracies. **(D – G)** Simulated and neural beta power lateralization data demonstrates collapsing bounds, whereby faster responses are made at higher thresholds. Shades in **F** and **G** represent 99.9% CI, the vertical blue and orange lines in **F** and **G** reflect mean target onset per condition. Grey backgrounds in **G** indicate significant time-points after Bonferroni correction. In **F** we rectified the modeled diffusion signal to always plot the unchosen response up and the chosen response down. For details about the simulation see Methods. **(B - C)** boxes = interquartile range (IQR), o = median, - = mean, whiskers =1.5 × IQR, grey dots = outlier

Cortical beta power lateralization reflects neural implementation of decision boundary collapse

Next, we tested the hypotheses that response-locked peak BPL represents a neural implementation for decision boundary collapse. First, we confirmed that beta power decreased more at centro-parietal electrodes contralateral to the initiated response (see Supplementary Figure 2), suggesting that BPL reflects differential motor activation. When averaged across trials in a median-split analysis, differences in BPL are clearly evident in the response locked data, where fast responses show a higher BPL (i.e., higher decision boundary; fast RT: -0.13 (SD: .003) vs. slow RT: -0.10 (SD: .003); $t(862) = -9.58$, $p < .001$, $d = 0.25$, $BF_{10} = 3.09e^{+17}$, see Figure 1F). Thus, collapsing boundaries are confirmed by response-locked BPL, indicating that humans make use of a discounting function to decide earlier to fulfil a time criterion. To confirm this finding on a single-trial level we regressed task-related behavioural factors onto measured individual single-trial BPL at response execution (button press ±12ms). This allows to control for other task factors that may additionally influence BPL but are not of primary interest for this short report. The regression analyses confirmed that BPL was

decreased (i.e., boundary collapse) for slower RTs ($t(862) = 12.74$, $p < .001$, $d = 0.43$, CI [0.42, 0.58], $BF_{10} = 6.14e^{+30}$, see Figure 3A). Plotting the RT quantiles against the BPL at response execution confirms a boundary collapse that closely resembles a sigmoidal function (Figure 3B). In an explorative analysis, we split the regression analysis by ipsilateral (hemisphere that does not induce the choice on the current trial) and contralateral hemispheres to better understand which hemisphere drives RT related BPL decreases (see Figure 3C). Results indicate that threshold decreases are partly due to slightly stronger decreases in beta power over the contralateral hemisphere (contralateral: $t(862) = 5.13$, $p < .001$, $d = 0.17$, CI [.19, .42], $BF_{10} = 1.57e^{+4}$ vs. ipsilateral: $t(862) = -3.68$, $p < .001$, $d = 0.12$, CI [-.33, -.10], $BF_{10} = 32.10$). However, the effect is stronger when the relative signal per trial is investigated, than when either of the hemispheres beta power is analyzed alone (contrast contralateral against BPL effect: $t(862) = 3.87$, $p < .001$, $d = 0.23$, $BF_{10} = 63.47$). These data suggest that peak BPL, coinciding with the motor response, may be an especially valid marker of response threshold modulations. However, it should be noted, that this assumption may be limited to speeded forced-choice tasks with short reaction times and evidence accumulation (Rogge et al., 2022).

Taken together, our results extend previous work on BPL as a neural signal that carries important features of a decision variable (Donner et al., 2009; Fischer et al., 2018). Particularly, BPL confirms the neural plausibility of dynamic DDMs that assume collapsing decision boundaries to terminate decision-formation under high time pressure. These results provide contrasting evidence to other human and animal studies who used other decision-making task (Hawkins, Forstmann, et al., 2015; Hawkins, Wagenmakers, et al., 2015; Roitman & Shadlen, 2002) and highlight that decision policies may not be generalized across tasks.

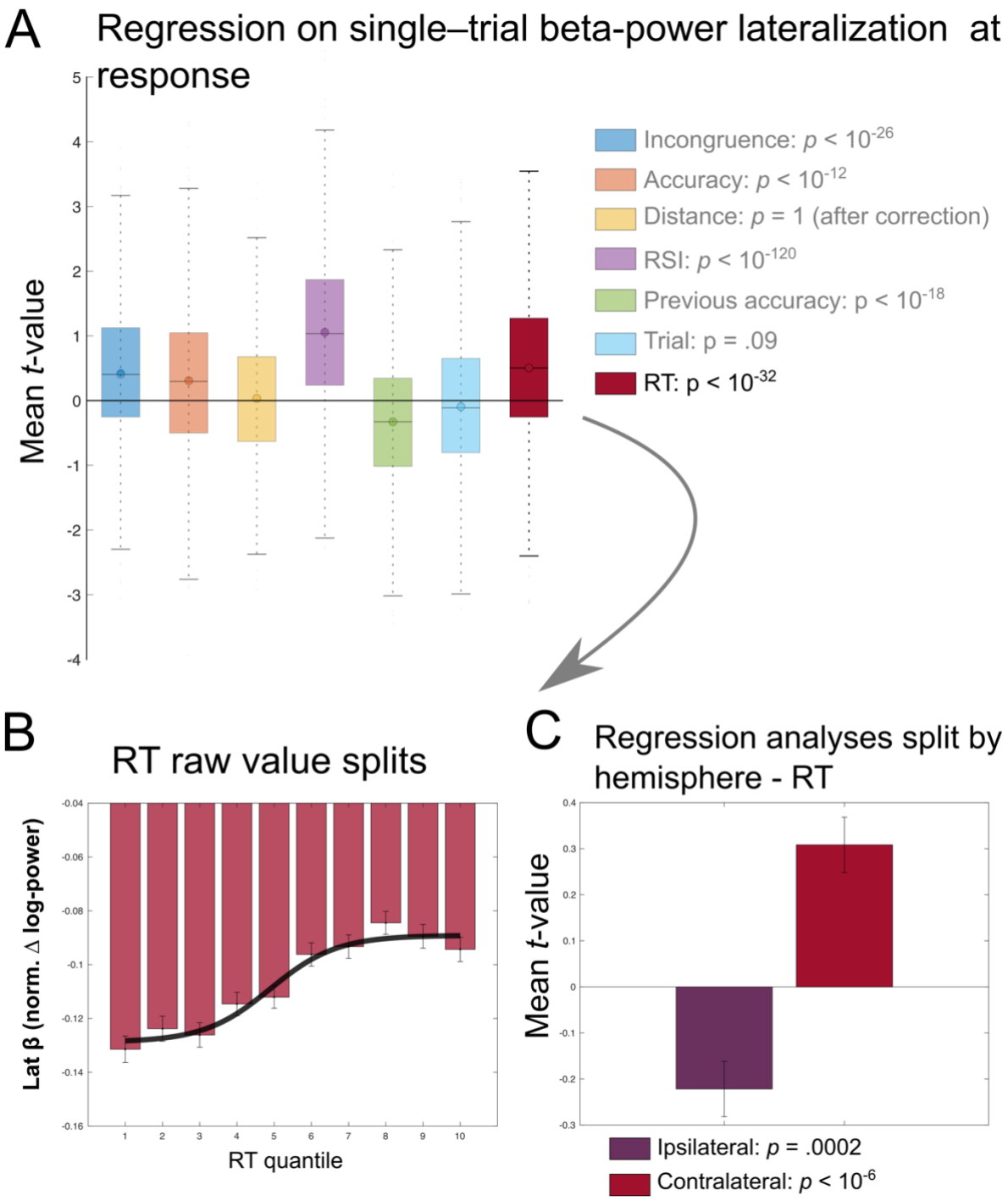

Figure 3. Single-trial regression on beta-power lateralization at response.

(A) Results of a single-trial regression analysis on BPL at response (mean ± 12ms surrounding button press). This analysis confirms collapsing decision boundaries on a single-trial level while controlling for other task factors that potentially influence BPL. **(B)** BPL raw values for RT quantiles plotted against BPL at response. Fitting the mean values trajectory confirms boundary collapse that closely resembles a sigmoidal function (black line expressed with: ymin = -0.13, ymax = -0.09, x0 = 4.89, and slope = 0.49, adjusted R^2 = .95). **(C)** Display results of separate regression analyses on beta power split by

(Figure 3 continued) ipsilateral (hemisphere that does not induce the choice on the current trial) and contralateral hemispheres. RT related BPL decrease is partly due to slightly more decreases over the contralateral hemisphere. **(A)** boxes= interquartile range (IQR), o = median, - = mean, whiskers =1.5 × IQR, grey dots = outlier. Error bars reflect standard error of the mean.

Materials and methods

Participants

Eight hundred ninety-five healthy young adults were recruited into the study. After exclusion of participants due to low task performance, recording failures, or poor data quality, 863 participants remained for subsequent analyses. The mean age of the sample including 434 female and 429 male participants was 24.2 years (range: 18–40). A detailed description of the sample characteristics and exclusion criteria can be found in Fischer et al. (2018).

Task

We employed a speeded arrow version of the Eriksen flanker paradigm in that participants were encouraged to respond as quickly and correctly as possible to the direction of the target arrow presented in the centre of the screen. The target could point either to the right or the left side, requiring a corresponding response with the right or left thumb. We additionally modulated response-stimulus intervals (short = 250ms, long = 700ms) as well as the distance between the imperative central and distracting flanker arrows (far distance: 6.5° and 4°, and close 3.5° and 1.75° visual angle). In total the task comprised 1,080 trials (see Fischer et al 2018, for more details on the task). A short response window of 1200ms and short RSIs ensured high-time pressure.

Drift-diffusion model and model comparison.

Features of the multi-stage sequential sampling models one to three, and general fitting procedures were exactly as described by Fischer et al. (2018). The description is adapted from therein. We used a multi-stage sequential sampling model to simulate participants' RT and accuracy distributions and the decision process giving rise to these. This discrete diffusion model simulates decisions as a Wiener process with stepwise increments according to a Gaussian distribution with mean ***v*** (called drift rate) and variance ***s*** on every trial. Here, **v** reflects the speed of evidence accumulation and ***s*** the system's noise, which scales all other parameters and is usually fixed (here to 0.1). The step size for all models was set to 1ms. Responses are triggered when the diffusion reaches a criterion (boundary, determined by the free parameter ± ***a***). We assumed that there was no bias in response selection over the task, because we had an equal number of left and right responses. However, individual trials were allowed to start with a random bias towards one response (start-point variability, parameter ***sz***). We used symmetrical boundaries which were defined as left-hand responses when the positive boundary was reached first, and as right-hand responses when the negative boundary was reached first (see Figure 1B for more details). The non-decision time was modelled as another free parameter $\boldsymbol{T_{er}}$. The stages of the model per trial were defined as a zero-mean baseline until flanker onset, a noisy diffusion with v = 0 during the non-decision time, a diffusion driven by the flanker direction between flanker and target onset (83 ms) with drift = vt × ft, and the target phase thereafter with drift = ***vt*** and the direction of the target. Single-trial values ***vt*** and ***ft*** were determined according to Gaussian variance parameters ***sv*** and ***sf***. For display purposes, in Figure. 2F, we modelled a consecutive return of the decision variable to baseline similar to an Ornstein-Uhlenbeck process to facilitate comparisons between model and BPL. To speed up the model fitting procedure, we did neither simulate baseline periods nor return to baseline during the fitting because these have no effect on

model predictions. We compared four different variants of the DDM by fitting their parameters to RT and accuracy data observed in the group of 863 participants using quantile maximum likelihood statistics (Heathcote et al., 2004) and differential evolution algorithms (Price et al., 2005). Additionally, we used a mixture model assuming 2% outliers that were distributed uniformly over the full range of RTs in correct and error responses. This downweighs the impact of possible outliers on model parameters. DDM model 1 used the same drift rate during flanker and target processing, thus not allowing for suppression of distractors (parameter ***f*** fixed to 1). DDM model 2 fixed parameter ***f*** which suppressed flanker processing when below the value of 1. DDM model 3 furthermore included trial-by-trial variance in ***f*** modelled as a zero-mean Gaussian distribution with variance ***sf***. The fourth DDM model extended DDM model 3 to allow for a dynamic decision boundary collapse according to a Weibull distribution scaled by the free parameter ***k***. Here, the dynamic boundary ***u*** at time ***t*** was calculated as follows:

$$u_t = a - \left(1 - \exp\left(\frac{t}{k}\right)^s\right) * a$$

In this equation, $\boldsymbol{a}$ represents the initial boundary value and $\boldsymbol{k}$ scales the Weibull distribution. The shape parameter $\boldsymbol{s}$ was fixed at 3, to impose a “late collapse” decision strategy. This value/shape was informed by results from a previous study in a large human sample (Hawkins, Forstmann, et al., 2015).

For model comparison, we first computed approximated BIC values (aBIC; akin to White et al. (2011)). Next, we used these individual aBIC values to computed protected exceedance

probabilities, which gives the probability that one model was more likely than any other model of the model space (Rigoux et al., 2014).

To simulate the temporal evolution of the modelled diffusion signal depicted in Figure 3 we used the mean maximum likelihood parameters from the group fit obtained for DDM 4. For this simulation, we computed 5000 simulated trials.

EEG processing

EEG was recorded at 500Hz from 60 Ag/AgCl sintered electrodes with A1 as reference channel and an electrode placed over the sternum as the ground electrode arranged in the extended 10-20 system using BrainAmp amplifiers (Brain Products, Gilching, Germany). Impedances were kept below 5 kΩ. Pre-processing of the EEG data was done under Matlab 2021b (The MathWorks, Natick, MA) and the EEGlab 13 toolbox (Delorme and Makeig, 2004) using custom routines as described previously (Fischer et al., 2018). Pre-processing steps included: (1) Filtering (0.5 Hz high- and 42 Hz low-pass filter), (2) re-referencing to common average, (4) Segmentation into stimulus-locked epochs spanning −1.5 to 2 s relative to target onset, (5) automatic epoch rejection. Here, epochs contaminated with artefacts were rejected using a dynamically adjusted rejection threshold to remove at least 1 trial separately for error and correct responses and maximally 5% per condition (average number of rejected epochs: 41, range 11–53). (6) removal of blink, eye-movement, and other, less homogenous artefact components (average number of removed components = 3.4, range 1–14) using adaptive mixture independent component analysis (AMICA; Palmer et al., 2012). Finally, we extracted response-locked epochs spanning from −1 to 1 s from the stimulus-locked epochs.

EEG analyses

First, we convolved the artefact free response-locked EEG signal, with a series of complex Morlet wavelets between 13 and 25 Hz. We used 20 linear steps and a wavelet width of six cycles. Data were then log-transformed and normalized. When comparing the averaged signal over contralateral (electrodes C3/CP3 for right and C4/CP4 for left) and ipsilateral (electrodes C3/CP3 for left and C4/CP4 for right) motor cortices, we show an overall decrease in beta power around 300ms prior to the response, which was followed by a consecutive increase in beta power (i.e., beta rebound) around 400ms post response (Supplementary Figure 2 a). To confirm the lateralisation of the signal to the hemisphere initiating a response, we used single-trial multiple robust regression. Here, we regressed the factor response hand (-1 = left, 1 = right) onto the convolved signal across the collapsed frequency range of 13–25 Hz for every electrode and time point, while controlling for unspecific task effects. Noise-Regressors included: congruency, flanker distance, RSI, following RSI, trial number, and log transformed RT. This analysis confirmed response related beta band lateralisation, whereby beginning around 100ms before response onset, beta power decreased over the sensorimotor cortex contralateral to the response. This was reflected in a positive covariation between response hand and the signal in the beta band which was maximal at C4/CP4, and a negative covariation at maximal at C3/CP3 (Supplementary Figure 2). We chose electrodes with a maximal effect (C3, C4, CP3, CP4) for all further analyses of lateralised beta power (BPL).

To derive BPL we subtracted beta band power over the inactive sensorimotor cortex (i.e., the electrodes side ipsilateral to the hand that gave the response in the trial) from the beta power recorded over the active (contralateral) sensorimotor cortex. This difference signal thus compares the degree of beta power reduction between both hemispheres, presumably reflecting differential motor activation (Supplementary Figure 2). To investigate

single-trial associations of beta thresholds and RT, we used the response-locked single-trial signal (mean ± 12 ms) and regressed the log-transformed RT onto the beta threshold while accounting for unspecific task effects according to the following equation:

$$BPL\ Threshold\ =\ b_0 + b_1 * Congruency + b_2 * Accurancy + b_3 * RSI + b_4 * Previous\ Accurcay + b_5 * Trial + b_6 * \log(RT) + e$$

In an explorative analysis, we used the same model to test the separate contributions of each hemisphere (ipsilateral and contralateral beta power).

Data and code availability

The conditions of our informed consent form do not permit public archiving of the raw data because participants did not provide sufficient consent. Researchers who wish to access processed and anonymized data from a reasonable perspective should contact the corresponding author. Data will be released to researchers if it is possible under the terms of the GDPR (General Data Protection Regulation). The code of the toolbox we used for the regression analysis can be found here: http://www.adrianfischer.de/teaching.html. The code for the DDM models is available on request.

Acknowledgments

This research was supported by the Deutsche Forschungsgemeinschaft (KL 2337/2-1 to TAK, UL 196/3-3 to MU) and by the European Research Council (ERC) under the European Union's Horizon 2020 research and innovation programme (ERC advanced grant agreement No 101018805 to MU).

Declaration of Competing Interest

The authors declare no conflict of interest.

References

Cisek, P., & Kalaska, J. F. (2005). Neural correlates of reaching decisions in dorsal premotor cortex: specification of multiple direction choices and final selection of action. *Neuron*, *45*(5), 801-814. https://doi.org/10.1016/j.neuron.2005.01.027

Danielmeier, C., & Ullsperger, M. (2011). Post-error adjustments. *Front Psychol*, *2*, 233. https://doi.org/10.3389/fpsyg.2011.00233

Danielmeier, C., Wessel, J. R., Steinhauser, M., & Ullsperger, M. (2009). Modulation of the error-related negativity by response conflict. *Psychophysiology*, *46*(6), 1288-1298. https://doi.org/10.1111/j.1469-8986.2009.00860.x

Donner, T. H., Siegel, M., Fries, P., & Engel, A. K. (2009). Buildup of choice-predictive activity in human motor cortex during perceptual decision making. *Curr Biol*, *19*(18), 1581-1585. https://doi.org/10.1016/j.cub.2009.07.066

Fischer, A. G., Nigbur, R., Klein, T. A., Danielmeier, C., & Ullsperger, M. (2018). Cortical beta power reflects decision dynamics and uncovers multiple facets of post-error adaptation. *Nat Commun*, *9*(1), 5038. https://doi.org/10.1038/s41467-018-07456-8

Hanks, T. D., & Summerfield, C. (2017). Perceptual Decision Making in Rodents, Monkeys, and Humans. *Neuron*, *93*(1), 15-31. https://doi.org/10.1016/j.neuron.2016.12.003

Hawkins, G. E., Forstmann, B. U., Wagenmakers, E. J., Ratcliff, R., & Brown, S. D. (2015). Revisiting the evidence for collapsing boundaries and urgency signals in perceptual decision-making. *J Neurosci*, *35*(6), 2476-2484. https://doi.org/10.1523/JNEUROSCI.2410-14.2015

Hawkins, G. E., Wagenmakers, E. J., Ratcliff, R., & Brown, S. D. (2015). Discriminating evidence accumulation from urgency signals in speeded decision making. *J Neurophysiol*, *114*(1), 40-47. https://doi.org/10.1152/jn.00088.2015

Heathcote, A., Brown, S., & Cousineau, D. (2004). QMPE: estimating Lognormal, Wald, and Weibull RT distributions with a parameter-dependent lower bound. *Behav Res Methods Instrum Comput*, *36*(2), 277-290. https://doi.org/10.3758/bf03195574

Hunt, L. T., Woolrich, M. W., Rushworth, M. F., & Behrens, T. E. (2013). Trial-type dependent frames of reference for value comparison. *PLoS Comput Biol*, *9*(9), e1003225. https://doi.org/10.1371/journal.pcbi.1003225

Kuhn, A. A., Doyle, L., Pogosyan, A., Yarrow, K., Kupsch, A., Schneider, G. H., Hariz, M. I., Trottenberg, T., & Brown, P. (2006). Modulation of beta oscillations in the subthalamic area during motor imagery in Parkinson's disease. *Brain*, *129*(Pt 3), 695-706. https://doi.org/10.1093/brain/awh715

Palestro, J. J., Weichart, E., Sederberg, P. B., & Turner, B. M. (2018). Some task demands induce collapsing bounds: Evidence from a behavioral analysis. *Psychon Bull Rev*, *25*(4), 1225-1248. https://doi.org/10.3758/s13423-018-1479-9

Pape, A. A., & Siegel, M. (2016). Motor cortex activity predicts response alternation during sensorimotor decisions. *Nat Commun*, *7*, 13098. https://doi.org/10.1038/ncomms13098

Price, K., Storn, R. M., & Lampinen, J. A. (2005). *Differential Evolution*. Springer Science & Business Media,.

Purcell, B. A., & Kiani, R. (2016). Neural Mechanisms of Post-error Adjustments of Decision Policy in Parietal Cortex. *Neuron*, *89*(3), 658-671. https://doi.org/10.1016/j.neuron.2015.12.027

Ratcliff, R., Smith, P. L., Brown, S. D., & McKoon, G. (2016). Diffusion Decision Model: Current Issues and History. *Trends Cogn Sci*, *20*(4), 260-281. https://doi.org/10.1016/j.tics.2016.01.007

Rigoux, L., Stephan, K. E., Friston, K. J., & Daunizeau, J. (2014). Bayesian model selection for group studies - revisited. *Neuroimage*, *84*, 971-985. https://doi.org/10.1016/j.neuroimage.2013.08.065

Rogge, J., Jocham, G., & Ullsperger, M. (2022). Motor cortical signals reflecting decision making and action preparation. *Neuroimage*, *263*, 119667. https://doi.org/10.1016/j.neuroimage.2022.119667

Roitman, J. D., & Shadlen, M. N. (2002). Response of neurons in the lateral intraparietal area during a combined visual discrimination reaction time task. *J Neurosci*, *22*(21), 9475-9489. https://doi.org/10.1523/JNEUROSCI.22-21-09475.2002

Thura, D., & Cisek, P. (2017). The Basal Ganglia Do Not Select Reach Targets but Control the Urgency of Commitment. *Neuron*, *95*(5), 1160-1170 e1165. https://doi.org/10.1016/j.neuron.2017.07.039

White, C. N., Ratcliff, R., & Starns, J. J. (2011). Diffusion models of the flanker task: discrete versus gradual attentional selection. *Cogn Psychol*, *63*(4), 210-238. https://doi.org/10.1016/j.cogpsych.2011.08.001

Cortical beta power reflects a neural implementation of decision boundary collapse in a speeded flanker task

Kirschner et al.

Supplementary results

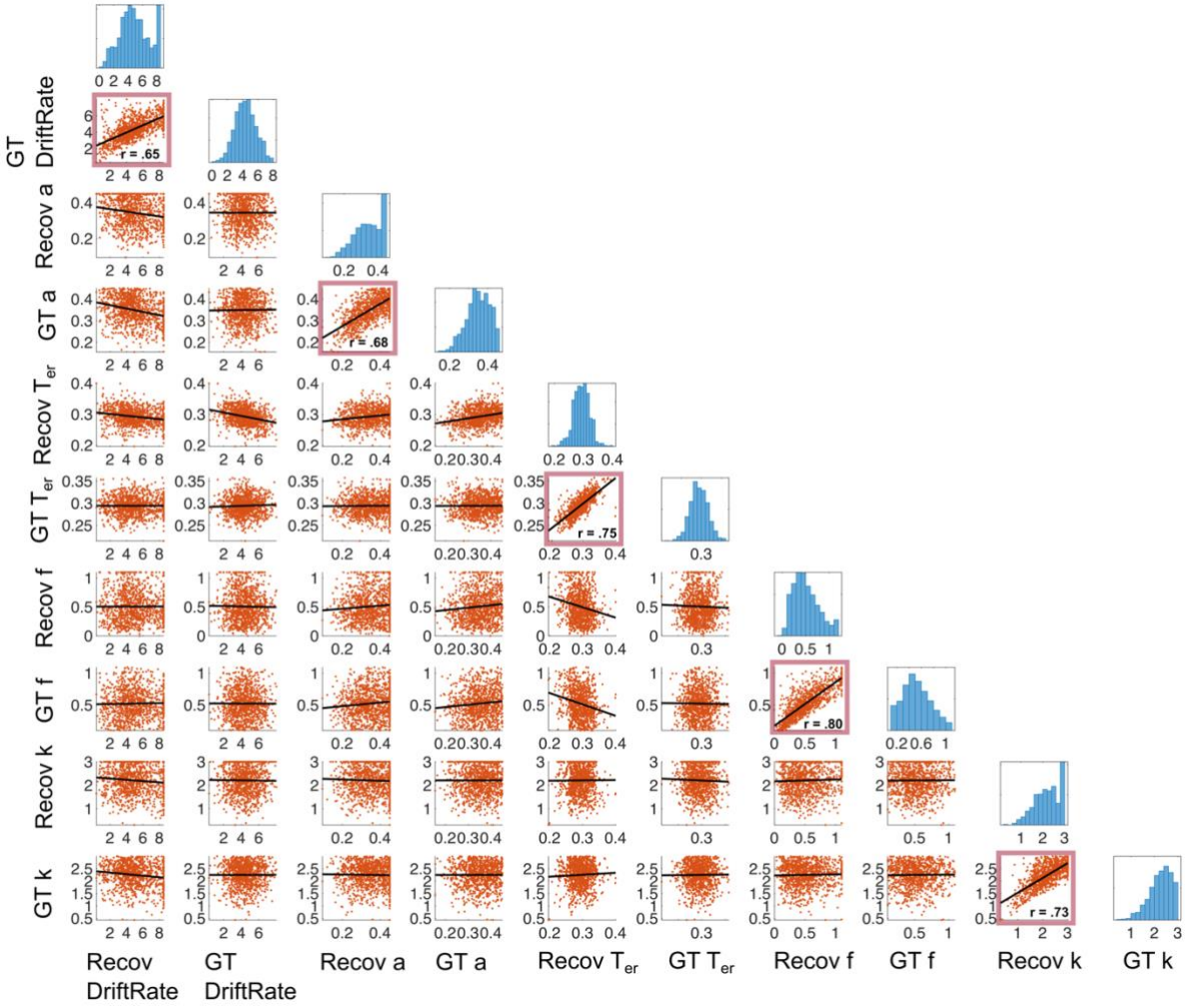

Supplementary Figure 1. Parameter recovery.

For parameter recovery analyses, we randomly drew model parameters out of a Gaussian distribution with mean and variance equal to the observed fitted parameters across the whole group to reduce parameter value combinations that were extremely unlikely to occur in human data. We simulated 1.000 parameter combinations and used the same differential evolution algorithm to recover the fitted models. Models that produced no errors at all or for which constraints were not met, were discarded from analysis. As in the human data, we used 5.000 trials per simulation. Plotted are ground truth (GT) parameters against the recovered parameters (plots marked in red frames). Additionally,

(Supplementary Figure 1 continued) we display the whole space of parameter combinations (maps without red borders) and distributions for each of the GT and recovered parameters. Overall, recovery studies indicate that drift-rate, response boundaries (a), non-decision time (T_{er}), flanker weighting (f), and boundary collapse (k) are independent and recoverable.

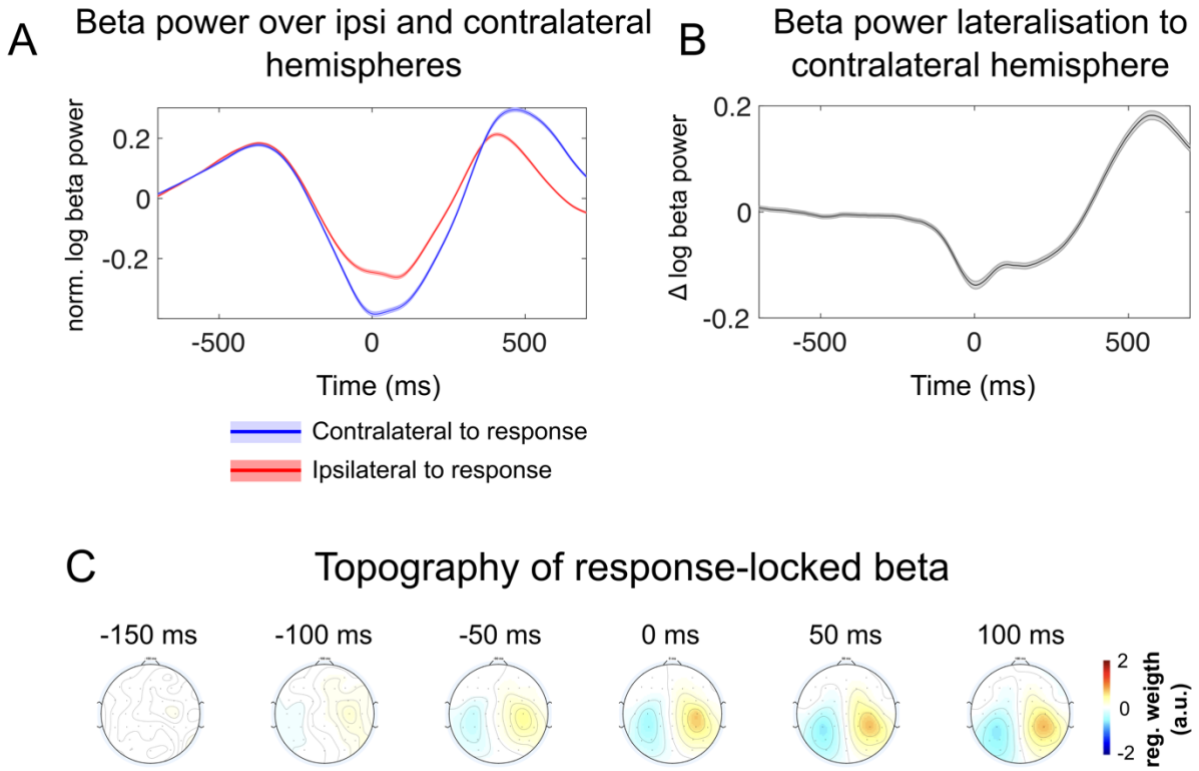

Supplementary Figure 2. Beta power and beta power lateralization.

Beta power lateralization **(B)** is composed of the activity-difference **(A)** recorded over contralateral (blue) and ipsilateral motor cortices (red). **(C)** shows the result of a single-trial regression analysis comparing responses with the left and right hand, while controlling for congruency, flanker distance, RSI, following RSI, trial number, and log transformed RT. Displayed are a regression weight maps of the scalp topography of beta power. Results confirms maximal effects at electrodes C3/4 and CP3/4 and suggest that Beta power more strongly decreases when a response is given with the contralateral compared to the ipsilateral hand.